Ti-substituted LaFeO$_3$ perovskite as photoassisted CWPO catalyst for water treatment

Patricia Garcia-Muñoz[a,*], Christophe Lefevre[b], Didier Robert[a], Nicolas Keller[a,*]

[a] *Institut de Chimie et Procédés pour l'Energie, l'Environnement et la Santé (ICPEES), CNRS/University of Strasbourg, 25 rue Becquerel, Strasbourg, France*
[b] *Institut de Physique et de Chimie des Matériaux de Strasbourg (IPCMS), CNRS/University de Strasbourg, 23 rue du Loess, Strasbourg, France*

A B S T R A C T

New Ti-substituted LaFeO$_3$ perovskites have been synthesized *via* a sol-gel method with partial substitution of La by Ti and used as catalyst in the photoassisted CWPO for the removal of 4-Cl-Phenol in water. The influence of the calcination temperature and the Ti at.% content was evaluated in terms of activity and stability. The Ti-substituted LaFeO$_3$ catalyst calcined at 800 °C showed an activity optimum for a 3.2 at.% content of Ti in the presence of the stoichiometric dose of H$_2$O$_2$, with a higher mineralization rate and yield than its LaFeO$_3$ counterpart, while achieving complete Cl-phenol removal and 100% mineralization at circumneutral pH, ambient pressure and temperature. The La partial substitution by Ti and the increase in the calcination temperature strongly improved the catalyst stability in terms of Fe leaching, and the Ti-substituted LaFeO$_3$ catalyst calcined at 800 °C displayed stable performances over 5 cycles of reaction, with a limited Fe leaching lower than 0.1% of its total content. The catalyst was active simultaneously in both photoassisted CWPO and photocatalysis under UV-A light. Thus, the photoassisted CWPO with Ti-substituted LaFeO$_3$ catalysts may overcome some drawbacks of single AOPs by combining higher rates at complete mineralization.

1. Introduction

Over the last decades, water treatment usually based on mechanical, physical, chemical or biological processes [1] had to face with the increase in both the volumes and the concentrations of polluted water streams, and in the decrease in biodegradability of the pollutants to be removed. In addition to the implementation of increasingly stringent and constraining environmental govern regulations, the heterogeneity of targets and of water matrix compositions and loads, as well as the emergence of biorecalcitrant pollutants has created a strong incentive for the development of new cost-effective, sustainable and high efficiency technologies or for the intensification of already existing technologies aiming at the abatement of pollutants in order to meet ever stricter legislation requirements.

Advanced Oxidation Processes (AOPs) have been successfully applied for the removal in water of a large panel of refractory compounds that are not degraded by conventional treatments [2–10]. These promising treatments are based on the generation of oxidative radicals HO$_x$° (HO° and HOO°) that react with the pollutant and subsequently with the reaction intermediates, leading to their oxidation and *in fine* to their removal from water. A wide variety of AOPs have been studied in detail such as, ozonation, photolysis, photocatalysis, Fenton process or

Catalytic Wet Peroxide Oxidation (CWPO), Catalytic Wet Air Oxidation (CWAO), …etc. Among them, the Fenton process, or its analogous heterogeneous CWPO, and photocatalysis, have gained special attention due to their high efficiency and relatively low cost [6].

Both processes operate through different reaction mechanisms and under different working conditions. In a typical Fenton process, the generation of HO$_x$° is achieved by the decomposition of H$_2$O$_2$ in the presence of metallic ions, in most of the cases iron. Despite a relatively high initial reaction rate, the Fenton AOP suffers mainly of the necessity to work at acidic pH and of the generation and precipitation of sludge due to the complexation of iron with short-chain acids. This results in a continuous loss of active phase and to the formation of wastes that strongly reduces the viability of the process. The heterogenization of the Fenton process by incorporating the active phase in a catalytic solid, known as CWPO, overcomes these issues, but decreases the process ability to achieve a complete mineralization of the pollutant an effluent and strongly reduces the reaction rates when compared to the homogeneous Fenton counterpart. Performing CWPO under light in the so-called photo-assisted CWPO or heterogenized photo-Fenton process is a promising strategy allowing the catalyst reactivity to be increased, although the constraints of acidic conditions and the incomplete mineralization are still important drawbacks [11,12].

---

* Corresponding authors.
E-mail addresses: garciamunoz@unistra.fr (P. Garcia-Muñoz), nkeller@unistra.fr (N. Keller).

By contrast, heterogeneous semiconductor photocatalysis is an AOP using the redox surface properties developed by an irradiated semiconductor material with adequate band gap for performing surface reactions between the adsorbed reactants and the $HO_X°$ oxidizing species produced from the electron and hole photogenerated charges. While the photocatalytic process can achieve a total mineralization of the refractory pollutants and enables working in a wide pH range value, it suffers unfortunately from far lower reaction rates than homogeneous AOPs like Fenton, and consequently from longer process durations [6].

Therefore, an approach for achieving simultaneously a higher reaction rate and a higher mineralization degree with no loss of active phase with time consists in the combination of both photo-assisted CWPO and photocatalysis processes. While physical mixtures of catalysts have been used [13–16], the design of a single phase catalyst enabling both processes to take place remains an interesting strategy scarcely investigated. The key-parameter remains that a unique catalyst needs to perform efficiently the decomposition of hydrogen peroxide into $HO_X°$ while acting simultaneously as heterogeneous photocatalyst under similar operating conditions.

In this frame, only few works have been reported on the combination of both photo-assisted CWPO and photocatalysis AOPs. $ZnFe_2O_4$ spinel ferrite was employed by Cai et al. [17] as visible light-assisted heterogeneous Fenton catalyst for the degradation of Orange II in water. While the photocatalyst displayed ability to split H_2O_2 and allowed a total Orange II removal with a low leaching of iron species (0.02%), only a 60% TOC removal was achieved. Similarly, Mechakra et al. [18] used natural iron oxide (containing mainly α-Fe_2O_3) for degrading the Linuron herbicide in water under UV and solar light, although only an 80% COD reduction was obtained at complete Linuron removal. Soltani and Lee reported that the heterogeneous photo-Fenton catalytic degradation of toluene in water under visible light led to 85% mineralization for a complete toluene removal under visible light on a Ba-doped $BiFeO_3$ perovskite with an optimum 0.12 Ba/Bi molar ratio [19]. Substitutional Ba within the perovskite structure improved the photo-Fenton catalytic degradation in weakly acidic conditions, due to the efficient redox cycling of iron species, and to the presence of abundant oxygen vacancies resulting from the distortion (or from the induced metastability) of the flexible perovskite structure when partially substituted. Also, Garcia-Munoz et al. proposed that the presence of both ilmenite and rutile semiconductor phases within a natural ilmenite mineral ($FeTiO_3$ with *ca.* 15% of rutile TiO_2) enabled to obtain higher rates and mineralization yields under solar light than those obtained in the separate processes, with a complete phenol and H_2O_2 conversion for a TOC conversion of 95%, with a negligible 0.5% iron leaching [20].

Lanthanum ferrite ($LaFeO_3$) perovskite is an interesting p-type semiconductor with a narrow band gap of 2.65 eV and one of the most common ABO_3 perovskite type oxides investigated for being applied as gas sensor, electrode for solid oxide fuel cells, optoelectronic and magnetic materials or heterogeneous catalysts [21]. The transition metal B-cation presents redox characteristics that allow significant mobility of oxygen, thus conferring activity in redox reactions [22] to the perovskite material. In addition, the material takes great advantage of its composition versatility, *i.e.* $A_{1-x}A'_xB_{1-y}B'_yO_{3\pm\delta}$ with the possibility of A-and/or B-cation partial substitution and the consequent geometric and charge constraints [22], for modifying its textural, structural and electronic properties, and consequently for tuning its redox and catalytic properties. Therefore, the incorporation of divalent or trivalent cations into La or Fe sub-lattices has been investigated. Cation-substituted ferrites have been mostly applied as photo-Fenton catalysts, using *e.g.* Cu-doped $LaFeO_3$, or Fe-, Mn-, Co- or Cu-based lanthanum perovskite, the Fe-based one being the most active in the oxidation of acetic acid in water [23,24]. $LaFeO_3$ and doped-$LaFeO_3$ perovskites were not extensively studied as photocatalysts [21,25]. The effect of the partial substitution of La with divalent Ca or monovalent Li ions [26,27], and of Fe with Zn or Mn [28,29] has been investigated. Parrino

et al. synthesized Cu-substituted $LaFeO_3$ with enhanced activity in the gaseous propanol degradation under solar light [25]. Although its low activity under visible light was improved through band-gap engineering by cation incorporation [27,30], the results remained far from complete mineralization, whereas $LaFeO_3$/AgBr, $LaFeO_3$/TiO_2 or $LaFeO_3$/SnS_2 heterojunction photocatalysts led very recently to enhanced performances under visible light compared to the bare $LaFeO_3$ photocatalyst, thanks to a Z-Scheme mechanism or to inter-conduction band electron transfer [15,31,32].

Here, we report for the first time on the synthesis *via* a simple sol-gel method of reusable Ti-substituted $LaFeO_3$ catalysts for use in water treatment, that combine both photo-assisted CWPO and photocatalysis processes in order to simultaneously improve the reaction rates and the TOC conversion at circumneutral pH conditions in comparison to the single AOP counterparts, while reducing the iron release into the water for improving the catalyst stability. The removal of 4-Cl-Phenol in water was selected as test reaction under UV-A light, since 4-Cl-Phenol is a model pollutant widely used in AOP studies as being representative of industrial wastewater refractory pollutants.
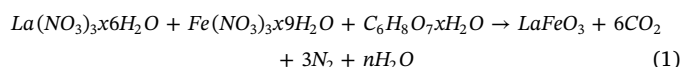
2. Materials and methods

2.1. Materials

Analytical grade chemicals were used without further purification. 4-Cl-Phenol (> 99%) and H_2O_2 (> 30%) were purchased from Sigma Aldrich. La$(NO_3)_3$ hexahydrate, Fe$(NO_3)_3$ nonahydrate and citric acid hydrate ($C_6H_8O_7xH_2O$,99.5%) were purchased from Sigma Aldrich. Commercial Aeroxide© TiO_2 P25 was obtained from Evonik.

2.2. Synthesis of Ti-modified $LaFeO_3$

Ti-modified $LaFeO_3$ materials were obtained by modifying a classical sol-gel Pechini synthesis. In this method, lanthanum nitrate hexahydrate and iron nitrate nonahydrate were dissolved in 30 mL distilled water at 108.3 g/L and 133 g/L, respectively, and the metallic ions undergo complexation by subsequent addition of citric acid at 70 g/L, corresponding to a stoichiometric molar ratio in respect of the metallic ions. Controlled amounts of TiO_2 Aeroxide P25 were further directly introduced under stirring into the aqueous sol, corresponding to nominal amounts of 5, 10, 15, 20, 30 and 50 wt.% in respect of the theoretical amount of $LaFeO_3$ perovskite obtained. The resulting suspensions were maintained at 80 °C for 2 days (2 °C/min heating rate) in order to induce the complete gel formation. The calcination of the dried gel was performed using a heating cycle as reported by Gosavi et al. [33] with heating rates of 5 °C/min, consisting in holding the temperature at 600 °C for 2 h, before to further maintaining a temperature plateau at 700 °C or 800 °C for 2 h if necessary.

Without considering the titania phase, the stoichiometric reaction forming the $LaFeO_3$ perovskite structure is as follows (Eq. (1)) [34]:

$$La(NO_3)_3 x6H_2O + Fe(NO_3)_3 x9H_2O + C_6H_8O_7xH_2O \rightarrow LaFeO_3 + 6CO_2$$
$$+ 3N_2 + nH_2O \quad (1)$$

Non-modified lanthanum ferrite powders were synthesized as reference materials by following the same protocol without any addition of titania, with a similar calcination procedure at 600–800 °C.

2.3. Characterisation techniques

X-ray diffraction (XRD) pattern have been recorded at room temperature in a θ/θ mode on a Brucker D8 Advance diffractometer equipped with a monochromatic copper radiation source ($K\alpha$ = 1.54056 Å) with a scan step of 0.02°. Some patterns have been investigated by Rietveld refinement with the Fullprof software for which the modified Thompson-Cox-Hasting function was chosen to

generate the line shape of the diffraction peaks. Instrumental broadening has been previously determined by measuring the scattering from corundum (NIST standard SRM 1976b) [35,36].

The surface area measurements were carried out on a Micrometrics Tristar 3000 using N_2 as adsorbent at $-196\,°C$ with a prior outgassing at $250\,°C$ overnight to desorb the impurities or moisture.

The iron and titanium contents in the catalysts were determined by Inductively coupled plasma optical emission spectroscopy (ICP-OES) carried out on an Optima 7000 DV spectrometer (Perkin Elmer).

X-Ray Photoelectron Spectroscopy (XPS) characterization was performed on a ThermoVGMultilabESCA3000 spectrometer (Al Kα anode at $h\lambda = 1486.6\,eV$). The energy shift due to electrostatic charging was subtracted using the adventious sp2 carbon C 1 s band at 284.6 eV. Contributions with Doniach–Sunjic shape [37] and a' S-shaped' Shirley type background [38] were used.

2.4. Typical reaction procedure

The experiments were carried out in a batch beaker-type glass reactor at atmospheric pressure, at room temperature and using H_2O_2 as main oxidant. 50 mg of catalyst was dispersed under stirring in a 100 mL aqueous solution of 4-chlorophenol at 25 mg/L concentration, corresponding to an initial organic carbon concentration of 14.8 ppm and to a catalyst load of 0.5 g/L. Prior to irradiation, the suspension has been stirred for 1 h in the dark to ensure the establishment of the adsorption/desorption equilibrium. After adding hydrogen peroxide at the stoichiometric concentration corresponding to a complete mineralization of the initial pollutant (125 mg/L), the suspension was exposed to a $60\,W/m^2$ irradiance UV-A light centered at 365 nm, provided by Philips 24 W/10/4 P lamps. At each time interval, 15 mL of solution has been sampled and then filtered through 0.20 μm porosity filter to remove the photocatalyst powder if any, before the concentration of 4-chlorophenol has been determined by UV–vis spectrophotometry by monitoring the disappearance of the main absorption peak at $\lambda = 224\,nm$ [39]. Total Organic Carbon measurements were performed using a Shimadzu TOC-L analyzer to determine the organic carbon load. Hydrogen peroxide concentration was measured by colorimetric titration using the $TiOSO_4$ method [40] and the Fe leached during time-course of reaction was quantified by the ortho-phenanthroline method [41].

3. Results and discussion

3.1. Catalyst characterization

The Fe and Ti atomic contents of the Ti-modified $LaFeO_3$ samples were obtained by elemental chemical analysis (Table 1). It confirmed the presence of titanium inside the materials, with an increase in the Ti at.% content from 2.1% to 14.8% when increasing the nominal TiO_2 wt. % content used for the synthesis from 5 to 50%. The increase in the Ti at.% content was accompanied by the concomitant decrease in the Fe at.% content from 23% for the Ti-free material down to 9.6%.

Fig. 1 shows the XRD patterns of the Ti-modified $LaFeO_3$ materials calcined at 600 °C, 700 °C and 800 °C. The profile Rietvelt refinement of the diffractograms of selected samples is shown in Fig. S1, while the refined cationic distribution in the $LaFeO_3$ structure and the crystallographic data of the refined samples are provided in Table 2 and Table S1, respectively. The XRD patterns of Ti-free materials displayed the most intense diffraction peaks at $2\theta = 22.6°$, $32.2°$, $39.7°$, $46.1°$, $57.4°$and $67.3°$ corresponding to the diffraction of the (100),(110), (111),(200),(210) and (220) planes of the $LaFeO_3$ phase, respectively. Further, whatever the titanium content and the calcination temperature, all the patterns could be indexed in the Pbnm orthorhombic unit cell of $LaFeO_3$ (see Table 2, Table S1 and Fig. S1). Only α-Fe_2O_3 in small amount was observed as extra phase in some samples, while no La_2O_3 was observed. For instance, the $LaFeO_3$-800 sample contained 10% of α-Fe_2O_3. The addition of the TiO_2 powder during the sol-gel synthesis

Table 1
Some physico-chemical properties of the Ti-modified $LaFeO_3$ catalysts.

Catalyst	Nominal content (% wt TiO_2)	Fe (at. %)[a]	Ti (at. %)[a]	Ti/Fe molar ratio	S_{BET} (m^2/g)[b]		dp^c (nm)	
					600 °C	800 °C	600 °C	800 °C
LFO	0	23.0	0.0	0	17	8	16	23
LFTi5	5	17.7	2.1	0.12	22	17	16	18
LFTi10	10	16.0	3.2	0.20	45	28	15	16
LFTi15	15	14.8	6.4	0.43	44	19	17	15
LFTi20	20	12.6	8.0	0.63	44	20	20	17
LFTi30	30	12.3	9.2	0.76	43	25	17	14
LFTi50	50	9.6	14.8	1.66	56	40	14	17

[a] The Fe and Ti at. % contents were determined by chemical analysis after a microwave-assisted acidic dissolution in aqua regia at 185 °C under autogenic pressure. ICP-OES was carried out on an Optima 7000 DV spectrometer (Perkin Elmer) at the Analysis Platform of IPHC-Strasbourg, France.

[b] The Brunauer–Emmett–Teller (BET) specific surface area has been calculated from the N_2 adsorption isotherm.

[c] Derived from XRD pattern, as the average size of the coherent diffraction domains, calculated from the Scherrer equation applied on the most intense (1 1 0) plane diffraction peak with the usual assumption of spherical crystallites.

did not result in the presence of any anatase or rutile TiO_2 extra phases in addition to the Ti-substituted $LaFeO_3$ structure. During the calcination treatment, a solid-solid diffusion might occur between the TiO_2 crystallites of the Aeroxide P25 and the amorphous $LaFeO_3$ crystallites before they crystallize, allowing the titanium atoms to be distributed within the $LaFeO_3$ crystallites.

Further, the determination of the cationic distribution within the structures was performed considering that Ti can move to both cationic sites. The Ti/Fe and Ti/La occupations were then separately refined and refinements are presented in Table 2. It has been evidenced that Ti preferentially occupies the La site, so that the materials could be labelled as $La_xTi_yFeO_3$. This behavior is rather surprising since La is much bigger than Fe. Similar results were observed by Hou et al. with the substitution of the small size Li^+ ion into the La-sites of $LaFeO_3$ [27] prepared by sol-gel in the presence of acetic acid, and by Li et al. in the reverse emulsion synthesis of $La_{1-x}Ca_x^{2+}FeO_3$ catalysts [26]. By contrast, Cu^{2+} preferentially occupied the Fe^{3+} sites in Cu-doped $LaFeO_3$ prepared by hydrothermal or citrate autocombustion synthesis [24,25], while partial substitution of La by Ag and of Fe by Co was achieved in $LaFeO_3$ [42]. An increase in the La-to-Ti substitution ratio was observed with the increase in the nominal TiO_2 content, as well as with the increase in the calcination temperature (Table 2). However, the XRD patterns also revealed that the partial substitution of La by Ti led to an increase in the amorphous content of the catalyst.

The partial substitution resulted in a significative increase in the surface area of the material, whatever the calcination temperature, with *e.g.* surface areas in the $17–40\,m^2/g$ range at 800 °C *vs.* $8\,m^2/g$ for $LaFeO_3$. Further, the Ti-substituted $LaFeO_3$ showed a better resistance to the crystallite growth with the increase in the calcination temperature. Indeed, the significant increase in the mean crystallite size observed for $LaFeO_3$, from 16 nm at 600 °C to 23 nm at 800 °C, was not observed in the case of Ti-substituted $LaFeO_3$, that maintained smaller mean crystallite sizes whatever the calcination temperature. Similarly, the doping of $LaFeO_3$ by Li or Cu ions was also reported to suppress the growth of large crystallites during the thermal treatments compared to the undoped counterparts [24,25].

The UV–vis absorbance spectra of different Ti- substituted $LaFeO_3$ catalysts is shown in Fig. S2. Whatever the Ti content, they displayed the usual pattern for $LaFeO_3$ materials [27,30], with a broad absorption band in the UV–vis range till wavelengths of about 600 nm. This indicated that Ti-substituted $LaFeO_3$ materials, similarly than the $LaFeO_3$ material, could potentially act as photocatalyst within this wavelength range.

The morphology of the Ti-substituted $LaFeO_3$ was affected by the Ti
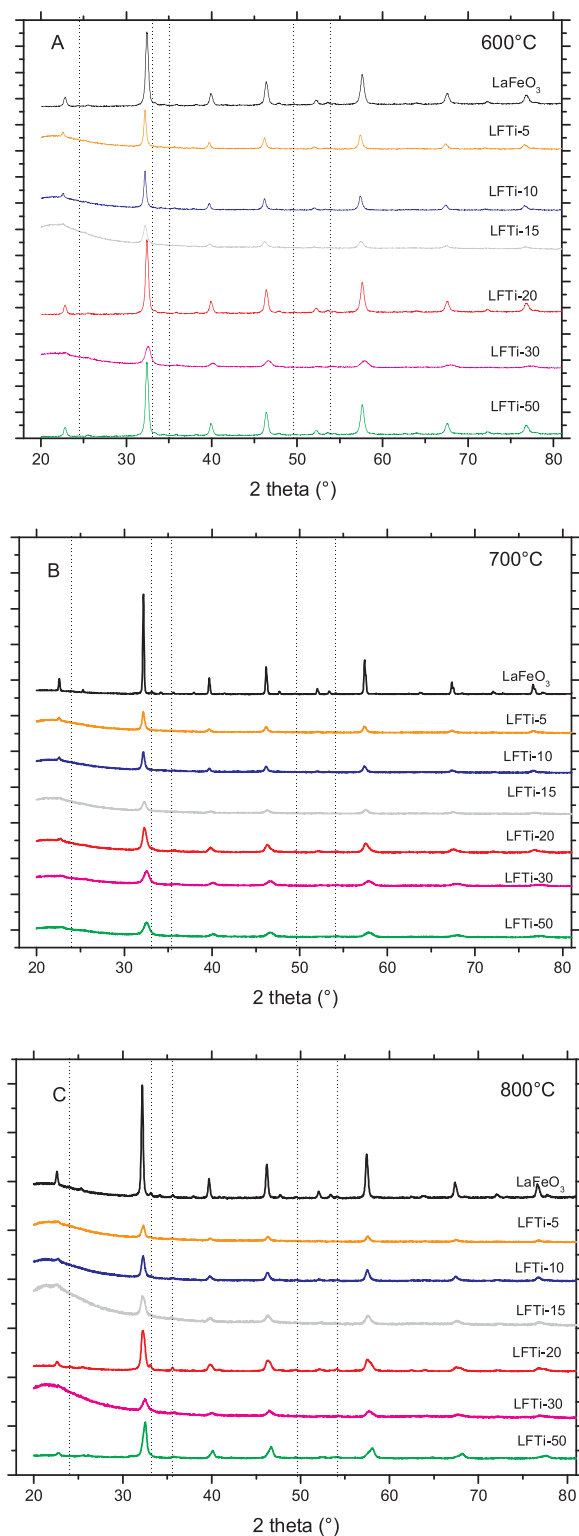
Fig. 1. XRD patterns of the Ti-modified LaFeO$_3$ materials calcined at (a) 600 °C, (b) 700 °C and (c) 800 °C. Dotted black lines corresponded to the main reflexes of the α-Fe$_2$O$_3$ extra phase formed in small amounts in some materials. LaFeO$_3$: JCPDS card 75-0541; α-Fe$_2$O$_3$: JCPDS card 01-089-8104.

content, as shown in the SEM images of Fig. S3. In the Ti-free material, the presence of well-defined grain boundaries of LaFeO$_3$ with a prismatic structure was evidenced (A–B), while the incorporation of titanium provoked an agglomeration of the structure (C–D), also responsible for an increase in the mesoporosity. This effect was all the

more pronounced that the titanium content was increased (E–F).

XPS analysis of the surface shown in Fig. S4 in the case of the pristine LFO-800 and of the LFTi10-800 catalysts evidenced that La and Fe species are present as La^{3+} and Fe^{3+} ions, whether the ferrite was modified by Ti or not. Indeed, on the pristine LaFeO$_3$ material, the La 3d core level spectra revealed the presence of a La 3d$_{5/2}$ - La 3d$_{3/2}$ orbital doublet contribution at 833.4 eV and 850.1 eV (spin orbit splitting of 16.7 eV [43–45] and multiplet splitting of 3.8 eV [46]), characteristic of La^{3+} species. Also, the presence of Fe in the formal oxidation state +3 was confirmed by the binding energies of Fe 2p$_{3/2}$ and Fe 2p$_{1/2}$ orbitals at 710.3 eV and 723.7 eV, with a 13.4 eV spin orbit coupling [46,47], together with the low intensity and broad shake-up satellite peak at about 718 eV characteristic of Fe^{3+} ions [48,49]. After substitution of La by Ti within the perovskite structure, the XPS Ti 2p orbital profile evidenced a single contribution, with the doublet related to Ti 2p$_{3/2}$–Ti 2p$_{1/2}$ spin-orbit components at 457.3 eV and 463.0 eV, characteristic of Ti species in lower oxidation state, and that might be assigned to Ti^{3+} substituting La^{3+} in the perovskite network [46]. It was worth nothing that this resulted also in a slight upward (+0.6–7 eV) and downward (−0.5 eV) shift of the La^{3+} and Fe^{3+} binding energies, respectively.

The upward shift observed for La^{3+} is characteristic of an electron deficiency induced by its chemical environment. Here, in La-O-Ti configurations, it might result from the O → Ti electron transfer (Ti being more electronegative than La), that would lead to shift the electronic density of the La-O bond towards the more electronegative oxygen atoms. Similarly, but in a mirrored reversed manner, the downward shift observed for Fe^{3+} in Fe-O-Ti configurations might result from the Ti → O electron transfer (Ti being less electronegative than Fe), that would lead to shift the electronic density of the Fe-O bond towards the less electronegative Fe atoms.

3.2. Catalytic activity

First, the performances of non-modified LaFeO$_3$ reference catalysts were evaluated for the degradation of 4-Cl-Phenol in water in absence and in presence of H$_2$O$_2$. Without H$_2$O$_2$, a very low photocatalytic activity was observed, and 42% of phenol removal with no TOC reduction was achieved in 240 min in the most efficient case using the LF-800 catalyst (Fig. S5). Further, Fig. 2A–L shows the evolution of 4-Cl-Phenol concentration, TOC, H$_2$O$_2$ decomposition and iron leached during the photo-assisted CWPO process performed on the LaFeO$_3$ catalysts and selected Ti-substituted LaFeO$_3$ catalysts. The results obtained with the complete La$_x$Ti$_y$FeO$_3$ catalyst series are reported in Fig. S8.

3.2.1. LaFeO$_3$ catalysts in the photo-assisted CWPO

Non-modified LaFeO$_3$ materials were first used as reference catalysts in the combined photo-assisted process. Whatever the calcination temperature, the pristine LaFeO$_3$ perovskite showed ability to decompose H$_2$O$_2$ in a typical photo-Fenton reaction (Fig. 2A-B-C). The LF-600 catalyst led to a total depletion of H$_2$O$_2$ in 120 min, with a Cl-phenol complete oxidation in 150 min and a mineralization rate of 85%. Both the LF-700 and LF-800 catalysts decomposed H$_2$O$_2$ slower than their LF-600 counterpart. Indeed, they needed about 300 min of reaction to achieve full H$_2$O$_2$ decomposition, while the complete phenol abatement was delayed to 210 and 150 min, respectively, with a TOC removal of 88% and 75%, respectively. The different behavior observed as a function of the calcination temperature could be related to the perovskite structure. The robustness of the material in terms of iron release to the water was influenced by the calcination temperature and the iron leaching was reduced from 2 mg/L at 600 °C down to 0.8 mg/L at 700 °C and 0.5 mg/L at 800 °C. The lesser robustness and the consequent lesser stability of the LF-600 catalyst was proposed to be responsible for the faster H$_2$O$_2$ decomposition. Nevertheless, the greater H$_2$O$_2$ decomposition rate did not result in a faster TOC disappearance which means small catalyst efficiencies as corroborated by the incomplete effluent

Table 2
Refined cationic distribution in the $La_xTi_yFeO_3$ perovskite catalysts and weight percentage of extra phases obtained after Rietveld refinement.

	La site distribution		Fe site distribution		%α-Fe₂O₃ (wt. %)	%TiO₂ (wt.%)
	La	Ti	Fe	Ti		
LFO-600	1	0	1	0	0	0
LFO-700	1	0	1	0	0	0
LFO-800	1	0	1	0	11	0
LFTi10-600	0.98	0.02	1	0	0	0
LFTi10-700	0.94	0.06	1	0	0	0
LFTi15-800	0.95	0.05	1	0	15	0
LFTi50-600	0.96	0.04	1	0	0	0
LFTi50-800	0.8	0.2	1	0	3	0
LFTi15-600_used	0.92	0.08	1	0	7	3
LFTi15-800_used	0.86	0.14	0.62	0.38	12	6

mineralization. On the other hand, the limited photocatalytic activity of those materials under UV-A light (Fig. S5) did not enhance the mineralization degree *vs.* the one obtained for photo-Fenton process.

3.2.2. CWPO reaction in the dark

Preliminary CWPO experiments performed on pristine and Ti-substituted LaFeO₃ evidenced the low oxidation ability of the catalysts in the dark (Fig. S6A–C for the catalyst series calcined at 800 °C). In the best case, the H_2O_2-assisted oxidation of 4-Cl-phenol only reached 40% after 360 min of reaction while a total H_2O_2 conversion was obtained, and very low and stable TOC mineralization yields within the 6–24% range were achieved. This typical CWPO behaviour was related to the
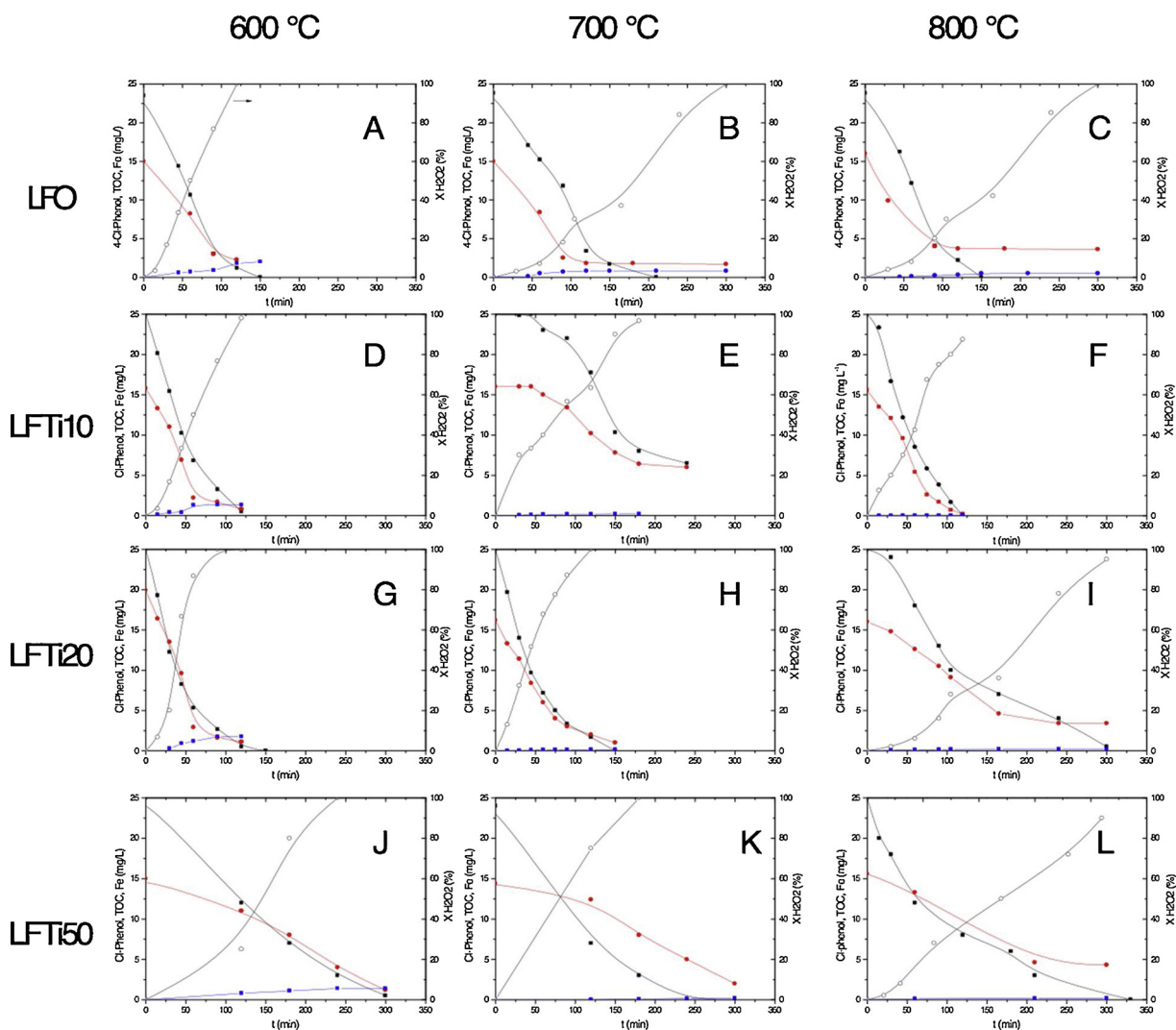

Fig. 2. Evolution of 4-Cl-Phenol (■), TOC (●), H_2O_2 decomposition (○) and iron leached (■) during the photo-assisted CWPO process over (A–C) the pristine LaFeO₃ catalysts and the Ti-substituted LaFeO₃ catalysts with TiO₂ nominal contents of (D–F) 10%, (G–I) 20% and (J–L) 50%. Operating conditions: [4-Cl-Phenol]₀ = 25 mg/L; [H₂O₂]₀ = 125 mg/L; T = 25 °C; [cat] = 0.5 g/L. The H_2O_2 and Cl-phenol concentration evolution curves were fitted by a pseudo first-order kinetic, and that of the TOC concentration with a zero-order kinetic model as usually admitted.

Table 3

Kinetic rate constants of H_2O_2 decomposition and Cl-Phenol oxidation, mineralization rate, Fe leached, H_2O_2 depletion percentage, TOC conversion and H_2O_2 efficiency parameters.

T(°C)/ %Ti	k_{H2O2} (min^{-1})	$k_{Cl\text{-}Phenol}$ (min^{-1})	$r_{0\,TOC}$ (mg/L min)	$[Fe]_{leached}$ (mg/L)	X_{H2O2} (%)	X_{TOC} (%)	ε_{H2O2}
600 °C/ LFO	0.018	0.021	0.11	2.0	100	85	0.85
LFTi5	0.015	0.022	0.12	1.7	100	87	0.87
LFTi10	0.019	0.023	0.13	2.0	100	98	0.98
LFTi15	0.015	0.022	0.11	1.5	100	83	0.83
LFTi20	0.007	0.025	0.12	1.6	100	98	0.98
LFTi30	0.007	0.012	0.05	1.5	100	88	0.88
LFTi50	0.008	0.008	0.03	1.4	100	96	0.96
700 °C/ LFO	0.012	0.022	0.11	0.8	100	88	0.88
LFTi5	0.010	0.020	0.16	0.4	100	85	0.85
LFTi10	0.008	0.013	0.15	0.2	100	80	0.80
LFTi15	0.007	0.013	0.14	0.1	100	84	0.84
LFTi20	0.007	0.011	0.15	0.2	100	98	0.98
LFTi30	0.009	0.012	0.05	0.3	100	85	0.85
LFTi50	0.009	0.011	0.03	0.2	100	95	0.95
800 °C/ LFO	0.010	0.020	0.12	0.5	100	75	0.75
LFTi5	0.011	0.022	0.13	0.1	95	81	0.85
LFTi10	0.017	0.025	0.18	0.05	90	100	1.11
LFTi15	0.012	0.015	0.08	0.2	92	87	0.95
LFTi20	0.006	0.008	0.07	0.2	97	85	0.88
LFTi30	0.005	0.009	0.07	0.1	95	87	0.92
LFTi50	0.005	0.007	0.05	0.2	98	80	0.82

large generation of short-chain acids (formic, oxalic and acetic) during the process (Fig. S6C), known to stop the reaction due to the formation of highly stable iron complexes.

3.2.3. Ti-substituted LaFeO$_3$ catalysts calcined at 600 °C in the photo-assisted CWPO

First, the incorporation of Ti inside the LaFeO$_3$ catalysts did not inhibit the catalyst ability to decompose H_2O_2 into HO_X° radicals used to further oxidize the organic compounds. For the LFTi catalysts calcined at 600 °C (Fig. 2D-G-J), 100% of H_2O_2 decomposition was obtained whatever the iron content in the material. However, as expected, the lower the iron content, the slower the H_2O_2 decomposition. The apparent pseudo first-order kinetic rate constants of H_2O_2 decomposition evidenced the highest depletion rates for smaller Ti/Fe ratios, at 0.019 min^{-1} for LFTi10 *vs.* 0.007 min^{-1} and 0.008 min^{-1} for LFTi20 and LFTi50, respectively (Table 3). The evolution of the H_2O_2 conversion was directly related to the Cl-Phenol removal profile, that showed a faster abatement with catalysts with higher iron contents. Indeed, 120, 150 and 300 min were needed for the total degradation of the phenolic compound using LFTi10, LFTi20 and LFTi50 catalysts, respectively, whereas the apparent kinetic rate constant for Cl-phenol disappearance was decreased from 0.022 min^{-1} for LFTi10 down to 0.008 min^{-1} for LFTi50 (Table 3).

By contrast to both the phenolic compound and the H_2O_2 profiles, the TOC profiles were fitted by a zero-order kinetic model as usually occurs in photocatalytic processes. The mineralization rate obtained with the Ti-substituted catalysts displayed a maximum for the LFTi10 catalyst at $r_0 = 0.13$ mg/L min, before to substantially decrease with the increase in the Ti content, down to $r_0 = 0.03$ mg/L min for the highly loaded LFTi50 sample (Table 3). Despite the strong differences in terms of rate, all catalysts showed a high activity level with X_{TOC} values between 83% (for LFTi15) to 98% (for LFTi10 and LFTi20). The values of X_{H2O2} obtained with all the materials calcined at 600 °C corroborated that existence of additional reactions to decompose the peroxide (Table 3), total H_2O_2 conversions were achieved even when working at a high Ti/Fe ratio.
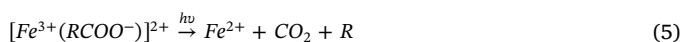
First, the H_2O_2 conversion profile can be influenced by additional surface as well as homogeneous reactions. Indeed, the adsorbed

peroxide can act as charge acceptor and be therefore reduced or oxidized by the photogenerated charges (e−/h+) issued from the perovskite (Eq. (2)) for forming HO_X° (HO° and HOO°) radicals (Eqs. (2)–(4)) [13]:

$$La_xTi_yFeO_3 \xrightarrow{h\nu} e^- + h^+ \tag{2}$$

$$e^- + H_2O_2 \rightarrow HO^\circ + OH^- \tag{3}$$

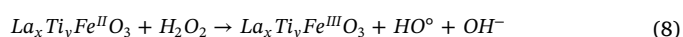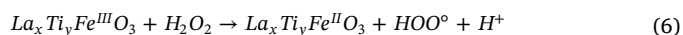$$h^+ + H_2O_2 \rightarrow HOO^\circ + H^+ \tag{4}$$

Secondly, the introduction of titanium inside the structure did not improve the stability of the material in terms of iron leaching when calcination is performed at 600 °C, with amounts of leached iron released to the solution of about 1.5–2 mg/L. Consequently, the low stability of the materials was responsible for the very probable strong contribution of the homogeneous Fenton process to the peroxide decomposition. These different reactions could provoke a different use of the oxidant, since the systems differed in terms of efficiency of the oxidant use, different mineralization yields being achieved. For instance, the reaction with LFTi5 obtained a $\xi = 0.87$ efficiency when 100% of peroxide was decomposed, while by contrast an efficiency of 0.96 was obtained for the same total peroxide conversion using the LFTi50 catalyst (Table 3).

Whatever the Ti/Fe ratio, no complete mineralization of the effluent was reached on catalysts calcined at 600 °C. This typical behavior of CWPO-like processes is associated to the presence of iron in solution, here resulting from the iron leaching. It has been reported that the iron in solution reacts with the latest oxidation intermediates, *e.g.* short-chain acids as oxalic acid, leading to the formation of iron-oxalate complexes [11,50]. These complexes are slower photodegraded which can confirm the incomplete TOC conversion obtained even in the presence of notable homogeneous Fenton contribution (Eq. (5)).

$$[Fe^{3+}(RCOO^-)]^{2+} \xrightarrow{h\nu} Fe^{2+} + CO_2 + R \tag{5}$$

3.2.4. Influence of the calcination temperature on the photo-assisted CWPO using Ti-substituted LaFeO$_3$ catalysts

Considering the increase in the catalyst robustness observed on the LaFeO$_3$ catalysts with a reduced Fe leaching when increasing the calcination temperature, a similar study was performed in the case of the La$_x$Ti$_y$FeO$_3$ catalysts (Fig. 2 and Fig. S8). Whatever the Ti content, the LFTi-700 catalysts achieved a total H_2O_2 decomposition within the first 180 min of reaction (Fig. 2E–K), with smaller k_{H2O2} than on LFTi-600 (Table 3). The catalyst stability was improved compared to that of LFTi-600, with a reduced iron release to the solution lower than 1 mg/L, and all the more reduced as the Ti content increased. Nevertheless, the amount of leached iron was still high enough to partially contribute with homogeneous photo-Fenton [51]. The evolution of Cl-Phenol concentration showed an induction period which was most pronounced at lower Ti content, especially when using the LFTi10-700 catalyst which showed a lag phase of around 120 min. This induction period has been associated to the Fe(III) to Fe(II) reduction by H_2O_2 and also by light effect as several authors has reported (Eqs. (6)–(8)) [20,52,53]. After the initial consumption of peroxide producing Fe(II), production of HO° can be achieved following Eq. (8). Over higher Ti content catalysts, the absence of any induction period for the 4-Cl-phenol concentration evolution might be ascribed to an additional photocatalytic contribution to the phenol degradation.

$$La_xTi_yFe^{III}O_3 + H_2O_2 \rightarrow La_xTi_yFe^{II}O_3 + HOO^\circ + H^+ \tag{6}$$

$$La_xTi_yFe^{III}O_3 \xrightarrow{h\nu} La_xTi_yFe^{II}O_3 \tag{7}$$

$$La_xTi_yFe^{II}O_3 + H_2O_2 \rightarrow La_xTi_yFe^{III}O_3 + HO^\circ + OH^- \tag{8}$$

The increase in the calcination temperature to 800 °C further improved the catalyst stability, with a substantial reduction of iron
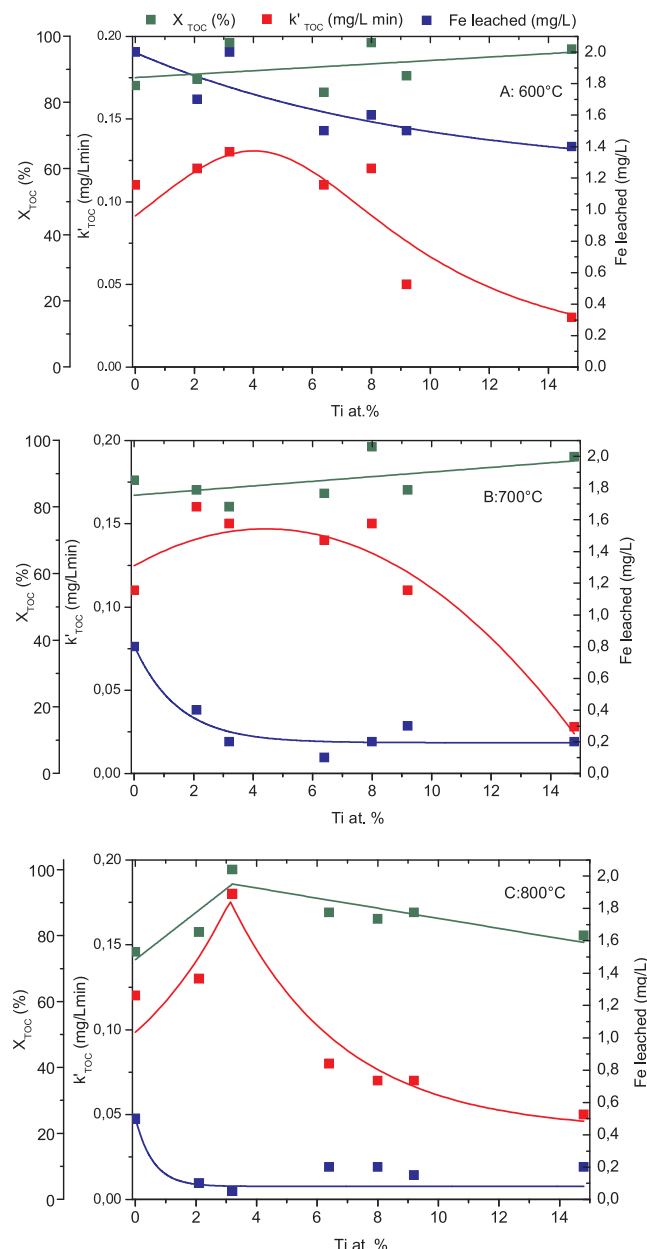
Fig. 3. Mineralization rate, TOC conversion and total iron leached at the end of photoassisted CWPO process as a function of the Ti at. % in the Ti-substituted LaFeO$_3$ catalysts calcined at: 600 °C (A), 700 °C (B) and 800 °C (C). Operating conditions: [4-Cl-Phenol]$_0$ = 25 mg/L; [H$_2$O$_2$]$_0$ = 125 mg/L; T = 25 °C; [cat] = 0.5 g/L. Trend curves have been drawn for visually evidencing the evolution profiles as a function of the Ti at.% content.

leaching, amounts of iron leached lower than 0.2 mg/L being detected whatever the Ti content. At this temperature, by contrast, 100% of H$_2$O$_2$ conversion was not obtained on the LFTi-800 catalysts, and the time required for achieving the final H$_2$O$_2$ conversion level increased as the Ti/Fe ratio increased (Fig. 2I–L). The time needed for the total removal of the phenolic compound increased from 120 min to 330 min with the increase in the Ti content from LFTi10 to LFTi50, respectively.

Fig. 3 shows the correlation between the activity, expressed in terms of apparent kinetic rate constant of TOC disappearance and mineralization degree, and the stability of the catalysts, expressed in terms of total iron leached from the solids. Whatever the calcination temperature, the kinetic rate constant displayed a volcano-like profile, centered around catalysts containing a 2.1–3.2 at.% content of titanium, while it strongly dropped down when further increasing the incorporation of

titanium. Increasing the temperature allowed to increase the maximum rate constant from 0.13 mg/L/min at 600 °C to 0.16 mg/L/min at 700 °C and further to 0.18 mg/L/min at 800 °C, overcoming in all cases the rate of 0.11-0.12 mg/L/min achieved on the non-modified bare LaFeO$_3$ catalysts.

Although some differences were observed, the TOC conversion was not strongly affected by the at.% content of titanium for materials calcined at 600 °C and 700 °C, and the TOC conversion remained at a high level, within the 83–98% and 80–98% range, respectively. By contrast, the incorporation of titanium inside the structure calcined at 800 °C led to a volcano-like profile for the TOC conversion, similar to that shown by the kinetic rate constant, a 100% mineralization degree being achieved with the Ti-substituted LaFeO$_3$ catalyst with 3.2 at.% of Ti.

Also, the incorporation of titanium inside the structure calcined at 600 °C led to reduce the iron leaching to the solution, from 2.0 mg/L for the non-modified LaFeO$_3$ catalyst down to 1.4 mg/L for a Ti at.% of 14.8. However, the iron leaching remained at a very high level of 1.4 mg/L for the Ti-rich perovskite structure, so that a pronounced contribution of homogeneous Fenton is expected. The positive effect related to the incorporation of titanium was more pronounced when increasing the calcination temperature, as evidenced by the Fe leached profile in Fig. 3B and C. This allowed to strongly reduce the contribution of homogeneous Fenton to the TOC conversion and the TOC removal kinetic rate constant.

Especially, the Ti-substituted LaFeO$_3$ catalyst calcined at 800 °C with 3.2 at.% of Ti. displayed a very good stability, with a negligible iron release of 0.05 mg/L to the solution that corresponded to 0.1% of its total iron content. As a result, the homogenous contribution could be considered as negligible and the higher mineralization rate at 0.18 mg/L with a final 100% TOC conversion only resulted from heterogeneous surface reactions. The heterogeneous mechanism was corroborated by comparing the CWPO-photoassisted reaction to the homogeneous photo-Fenton reaction performed with 0.05 mg/L of Fe^{3+} (Fig. S7). Indeed, despite 0.05 mg/L is the total Fe amount released at the end of the reaction in the case of the heterogeneous system and therefore remains higher than the real Fe amount during the main part of the process, and that the homogeneous system benefited from a maximum irradiation compared to the slurry reactor, the heterogeneous surface reaction contribution was overcoming by two orders of magnitude that of the homogeneous photo-Fenton process, with apparent 1st order kinetic rate constants of $2.5 \ 10^{-2}$ min^{-1} and $5.6 \ 10^{-4}$ min^{-1} for the Cl-phenol degradation, respectively.

Further, considering that a theoretical $\xi = 1$ efficiency of peroxide use in Fenton-like processes means that H$_2$O$_2$ and the formed radicals does not suffer from any detrimental scavenger reactions, this catalyst displayed a $\xi = 1.11$ H$_2$O$_2$ efficiency while achieving 100% TOC removal with a 90% H$_2$O$_2$ conversion. So, we proposed that the LFTi10-800 catalyst was active simultaneously in both photoassisted CWPO and photocatalysis. We cannot rule out that more generally the LFTi-800 catalysts with other Ti contents also showed a photocatalytic contribution to the degradation activity, since 100% H$_2$O$_2$ conversion was never achieved with this catalyst series.

The effect of partial substitution of La and/or Fe on the photocatalytic properties of the ferrite has been poorly described in the recent literature. Based on the recent works of Parrino et al. on Cu-substituted LaFeO$_3$ catalysts, we propose also that the superiority of the LFTi10-800 catalyst with optimal Ti substitution may result from the presence of oxygen vacancies [27]. They related the higher activity of the Cu-containing catalyst with an optimum at 10 at.% substitution rate with the presence of oxygen vacancies and with the reduced electron/hole recombination, evidenced through XPS analysis and transient photocurrent measurements. The cation substitution was reported to give rise to an electronic unbalance compensated by a change in the oxidation state of a part of the Fe(III), being oxygen vacancies formed to preserve the electroneutrality, and to adjust with the distortion of the anionic
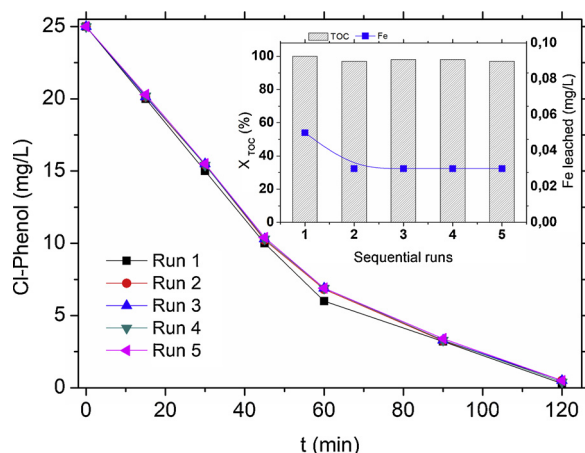
Fig. 4. Consecutive runs with reused LFTi10-800 catalyst. Operating conditions: [4-Cl-Phenol]$_0$ = 25 mg/L; [H$_2$O$_2$]$_0$ = 125 mg/L; T = 25 °C; [cat] = 0.5 g/L.

lattice [54]. An optimum in the substituted heteroatom content was also observed by Phan et al. in the degradation of dyes by heterogeneous photo-Fenton on Cu-substituted LaFeO$_3$ catalysts with 15 at.% Fe substitution by Cu ions [24]. Hou et al. also observed an optimum in the enhancement of the photocatalytic activity of Li-substituted LaFeO$_3$ catalysts, with 3 at.% of La substitution [27].

3.3. Stability tests of the LFTi10-800 catalyst in the photo-assisted CWPO

One of the main shortcomings of catalytic water treatments remains the stability of the catalysts, and the determination of the active phase release from the catalyst to the water during the process has to be completed with reusability tests for evidencing the catalyst stability. Fig. 4 shows the very good stability of the LFTi10-800 catalyst for five consecutive runs, with catalyst recovery by powder filtration. Apparent kinetic rate constants for the Cl-phenol disappearance of 0.23 ± 2 min^{-1} were obtained with the maintain after the run #5 of a global mineralization yield of 99% ± 1% after 120 min of reaction, while a residual loss of Fe of 0.03 mg/L was observed, corresponding to a 0.09% Fe release in respect to the Fe content of the catalyst.

However, the XRD pattern of Ti-substituted LaFeO$_3$ catalysts after test shown in Fig. S1D evidenced the formation during the reaction of rutile TiO$_2$ phase in very small amount (3–6%). However, this has no detrimental effect on the catalyst activity in terms of pollutant degradation and of TOC conversion, as well as on its stability in terms of iron leaching and of reusability. By contrast, we could not rule out that the formed TiO$_2$/La$_x$Ti$_y$FeO$_3$ heterojunction within the catalyst was beneficial for improving the photogenerated charge separation, as recently proposed for LaFeO$_3$-based heterojunction photocatalysts [15,31,32], with possible electron transfer from the perovskite conduction band to that of TiO$_2$ [15].

4. Conclusions

A series of novel Ti-substituted LaFeO$_3$ materials with varied titanium content have been synthesized *via* a simple sol-gel method using commercial TiO$_2$ as titanium precursor. The influence of the calcination temperature and of the titanium at.% content was evaluated upon both the activity in photoassisted CWPO under UV-A light and the stability of catalysts. The catalysts calcined at 600 °C suffered from the iron leaching resulting in notable homogeneous photo-Fenton contribution, while the activity of the catalysts calcined at 800 °C could be ascribed to heterogeneous surface reactions due to the increase in the catalyst stability with strongly reduced Fe leaching. The Ti-substituted LaFeO$_3$ catalyst calcined at 800 °C showed an optimum in activity for a 3.2 at.%

content of titanium, with a higher mineralization rate than the Ti-free LaFeO$_3$ counterpart, while achieving complete Cl-phenol removal and 100% mineralization at neutral pH over 5 cycles of reuse with stable efficiency and a limited Fe leaching lower than 0.1% of its total content. We proposed that this single-phase catalyst combined both photo-assisted CWPO and photocatalytic processes. Works are ongoing for increasing the material crystallinity and for taking advantage of its band gap value for operating the combined CWPO and photocatalysis process under visible light. In addition, further works will deal with the elucidation of the active species formed during the combined process, and with the use of the magnetic properties of the Ti-substituted LaFeO$_3$ materials for improving and simplifying the powder recovery process.

Appendix A. Supplementary data

Supplementary material related to this article can be found, in the online version, at doi:https://doi.org/10.1016/j.apcatb.2019.02.030.

References

[1] W. Xiong, G. Zeng, Z. Yang, Y. Zhou, C. Zhang, M. Cheng, Y. Liu, L. Hu, J. Wan, C. Zhou, R. Xu, X. Li, Sci. Total Environ. 627 (2018) 235.
[2] D.B. Miklos, C. Remy, M. Jekel, K.G. Linden, J.E. Drewes, U. Hübner, Water Res. 139 (2018) 118.
[3] D. Kanakaraju, B.D. Glass, M. Oelgemöller, J. Environ. Manage. 219 (2018) 189.
[4] M. Sillanpää, M.C. Ncibi, A. Matilainen, J. Environ. Manage. 208 (2018) 56.
[5] N. Serpone, Y.M. Artemev, V.K. Ryabchuk, A.V. Emeline, S. Horikoshi, Curr. Opin. Green Sustain. Chem. 6 (2017) 18.
[6] S. Malato, P. Fernández-Ibáñez, M.I. Maldonado, J. Blanco, W. Gernjak, Catal. Today 147 (2009) 1.
[7] C. Zhou, P. Xu, C. Lai, C. Zhang, G. Zeng, D. Huang, M. Cheng, L. Hu, W. Xiong, X. Wen, L. Qin, J. Yuan, W. Wang, Chem. Eng. J. 359 (2019) 186.
[8] P. García-Muñoz, G. Pliego, J.A. Zazo, B. Barbero, A. Bahamonde, J.A. Casas, Chem. Eng. J. 318 (2017) 89–94.
[9] H. Yi, D. Huang, L. Qin, G. Zeng, C. Lai, M. Cheng, S. Ye, B. Song, X. Ren, X. Guo, Appl. Catal. B Environ. 239 (2018) 408.
[10] Y. Yang, C. Zhang, D. Huang, G. Zeng, J. Huang, C. Lai, C. Zhou, W. Wang, H. Guo, W. Xue, R. Deng, M. Cheng, W. Xiong, Appl. Catal. B Environ. 245 (2019) 87.
[11] G. Pliego, J.A. Zazo, P. Garcia-Muñoz, M. Munoz, J.A. Casas, J.J. Rodriguez, Crit. Rev. Environ. Sci. Technol. 45 (2015) 2611.
[12] G. Pliego, P. Garcia-Muñoz, J.A. Zazo, J.A. Casas, J.J. Rodriguez, Environ. Sci. Pollut. Res. (2016) 1.
[13] M.E. Zarazua-Morin, L.M. Torres-Martinez, E. Moctezuma, I. Juarez-Ramirez, B.B. Zermeno, Res. Chem. Intermed. 42 (2016) 1029.
[14] A. Sivakumar, A. Selvaraj, A. Ramasamy, V. Balasubramanian, Water Air Soil Poll. 224 (5) (2013) 1529.
[15] R. Dhinesh Kumar, R. Thangappan, R. Jayavel, J. Phys. Chem. Solids 101 (2017) 25.
[16] S. Yu, Y. Wang, F. Sun, R. Wang, Y. Zhou, Chem. Eng. J. 337 (2018) 183.
[17] C. Cai, Z. Zhang, J. Liu, N. Shan, H. Zhang, D.D. Dionysiou, Appl. Catal. B 182 (2016) 456.
[18] H. Mechakra, T. Sehili, M.A. Kribeche, A.A. Ayachi, S. Rossignol, C. George, J. Photochem. Photobiol. A-Chem. 317 (2016) 140.
[19] T. Soltani, B. Lee, J. Mol. Catal. A-Chem. 425 (2016) 199.
[20] P. García-Muñoz, G. Pliego, J.A. Zazo, A. Bahamonde, J.A. Casas, J. Environ. Chem. Eng. 4 (2016) 542.
[21] K. Peng, L. Fu, H. Yang, J. Ouyang, Sci. Rep. 6 (2016) 19723.
[22] L. Hou, H. Zhang, L. Dong, L. Zhang, D. Duprez, S. Royer, Catal. Today 287 (2017) 30.
[23] D. Sannino, V. Vaiano, P. Ciambelli, L.A. Isupova, Catal. Today 161 (2011) 255.
[24] T.T.N. Phan, A.N. Nikoloski, P.A. Bahri, D. Li, J. Ind. Eng. Chem. 61 (2018) 53.
[25] F. Parrino, E. García-López, G. Marcì, L. Palmisano, V. Felice, I.N. Sora, L. Armelao, J. Alloys Compd. 682 (2016) 686.
[26] F. Li, Y. Liu, R. Liu, Z. Sun, D. Zhao, C. Kou, Mater. Lett. 64 (2010) 223.
[27] L. Hou, G. Sun, K. Liu, Y. Li, F. Gao, J. Sol Gel Sci. Technol. 40 (2006) 9.
[28] Z. Wei, Y. Wang, J. Liu, C. Xiao, W. Zeng, Mater. Chem. Phys. 136 (2012) 755.
[29] S. Dong, K. Xu, G. Tian, Photocatalytic Activities of LaFe$_{1-x}$Zn$_x$O$_3$ Nanocrystals

Prepared by Sol-gel Auto-combustion Method, (2009) p. 2548.

[30] S.K. Rashmi, H.S. Bhojya Naik, H. Jayadevappa, R. Viswanath, S.B. Patil, M. Madhukara Naik, Mater. Sci. Eng. B 225 (2017) 86.

[31] Y. Song, S. Xue, G. Wang, J. Jin, Q. Liang, Z. Li, S. Xu, J. Phys. Chem. Solids 121 (2018) 329.

[32] J. Luo, R. Li, Y. Chen, X. Zhou, X. Ning, L. Zhan, L. Ma, X. Xu, L. Xu, L. Zhang, Sep. Purif. Technol. 210 (2019) 417.

[33] P.V. Gosavi, R.B. Biniwale, Mater. Chem. Phys. 119 (2010) 324.

[34] X. Qi, J. Zhou, Z. Yue, Z. Gui, L. Li, Ceram. Int. 29 (2003) 347.

[35] L.B. McCusker, R.B. Von Dreele, D.E. Cox, D. Louër, P. Scardi, J. Appl. Cryst. 32 (1999) 36.

[36] J. Rodríguez-Carvajal, Physica B Condens. Matter 192 (1993) 55.

[37] M.S.S. Doniach, J. Phys. C Solid State Phys. 3 (1970) 285.

[38] D.A. Shirley, Phys. Rev. B 5 (1972) 4709.

[39] M. Pera-Titus, V. García-Molina, M.A. Baños, J. Giménez, S. Esplugas, Appl. Catal. B Environ. 47 (2004) 219.

[40] G. Eisenberg, Colorimetric determination of hydrogen peroxide, Industrial & Engineering Chemistry Analytical, (1943).

[41] E.B. Sandell, Colorimetric determination of traces of metals, J. Phys. Chem. 49 (1945) 263–264.

[42] V.R. Choudhary, B.S. Uphade, S.G. Pataskar, Fuel 78 (1999) 919.

[43] S. Phokha, S. Pinitsoontorn, S. Rujirawat, S. Maensiri, J. Nanosci. Nanotechnol. 15 (2015) 9171.

[44] S. Thirumalairajan, K. Girija, V. Ganesh, D. Mangalaraj, C. Viswanathan, N. Ponpandian, Cryst. Growth Des. 13 (2013) 291.

[45] M. Humayun, N. Sun, F. Raziq, X. Zhang, R. Yan, Z. Li, Y. Qu, L. Jing, Appl. Catal. B Environ. 231 (2018) 23.

[46] S. Petrović, A. Terlecki-Baričević, L. Karanović, P. Kirilov-Stefanov, M. Zdujić, V. Dondur, D. Paneva, I. Mitov, V. Rakić, Appl. Catal. B Environ. 79 (2008) 186–198.

[47] J. Faye, A. Baylet, M. Trentesaux, S. Royer, F. Dumeignil, D. Duprez, S. Valange, J. Tatibouët, Appl. Catal. B Environ. 126 (2012) 134.

[48] T. Yamashita, P. Hayes, Appl. Surf. Sci. 254 (2008) 2441.

[49] D.D. Hawn, B.M. DeKoven, Surf. Interface Anal. 10 (1987) 63.

[50] J.A. Zazo, G. Pliego, P. García-Muñoz, J.A. Casas, J.J. Rodriguez, Appl. Catal. B Environ. 192 (2016) 350.

[51] S. Papoutsakis, S. Miralles-Cuevas, N. Gondrexon, S. Baup, S. Malato, C. Pulgarin, Ultrason. Sonochem. 22 (2015) 527.

[52] K. Rusevova, F. Kopinke, A. Georgi, J. Hazard. Mater. 241–242 (2012) 433.

[53] R. Chen, J.J. Pignatello, Environ. Sci. Technol. 31 (1997) 2399.

[54] W. Lee, H.J. Yun, J. Yoon, J. Alloys Compd. 583 (2014) 320.